

Fluid-structure Interaction of Flexible Flapping Wings at High Altitude Conditions at Monarch Butterfly Scale

Madhu K. Sridhar¹, Chang-kwon Kang², David Brian Landrum³ University of Alabama in Huntsville, Huntsville, AL 35899

Hikaru Aono⁴

Tokyo University of Science, Tokyo, Japan

The long-range migration of Monarch butterflies extends over 4000 km. Monarchs experience varying density conditions during migration. Monarchs have been spotted at 1200 m during migration and overwinter at 3000 m, where the air density is lower than at the sea-level. Furthermore, Monarch butterflies have large flexible wings which deform significantly during flight. In this study, we test the hypothesis that the aerodynamic performance of the Monarch wing improves at reduced density conditions at higher altitudes. A design space with air density and stroke plane angle as design variables is constructed to evaluate the effects of fluid-structure interaction at high altitudes in the Reynolds number regime of $Re = O(10^3)$. The effects of chordwise wing flexibility and the aerodynamic and structural response at varying densities are investigated by solving the Navier-Stokes equations, fully coupled to a structural dynamics solver at the Monarch scale. The lift, thrust and power are calculated in the design space. Our results show that lift increases with the stroke plane angle and the air density, whereas the thrust remains close to zero. The mean power required reduces with the altitude, eventually becoming negative at 3000 m. These results suggest that at lower altitudes near sea level, Monarchs can leverage the relatively large magnitude of their lift and thrust forces. At higher altitudes butterflies can fly while minimizing the power.

I. Nomenclature

C_L	=	coefficient of lift, $C_L = L/0.5 \rho_f U^2 c_m$	[1]
$c_{ m m}$	=	mean wing chord	[m]
C_P	=	coefficient of power input	[1]
C_T	=	coefficient of thrust	[1]
E	=	elastic modulus	$[N/m^2]$
f	=	flapping frequency	[1/s]
f_1	=	first natural frequency of the wing	[1/s]
f/f_1	=	frequency ratio	[1]
F	=	fluid force acting per unit length	[N/m]
h	=	plunge motion	[m]
h	=	plunge velocity	[m/s]

¹ Graduate Student, Mechanical and Aerospace Engineering, Technology Hall C200, AIAA Student Member.

² Associate Professor, Mechanical and Aerospace Engineering, Technology Hall N266, AIAA Senior Member.

³ Associate Professor, Mechanical and Aerospace Engineering, Technology Hall N267, AIAA Associate Fellow.

⁴ Assistant Professor, Mechanical Engineering, 6-3-1 Niijyuku, Katsushika-Ku, Tokyo, Japan, AIAA Member.

$h_{\rm a}$	=	plunge amplitude, $h_a = \gamma_{p2p} R \hat{r}_2 / 4$	[m]
$h_{\rm s} h_{\rm s}^*$	=	membrane thickness	[m]
${h_{ m s}}^*$	=	thickness ratio, $h_s^* = h_s/c_m$	[1]
k	=	reduced frequency, $k = \pi f c_m / U$	[1]
L	=	lift	[N]
m_{w}	=	butterfly forewing mass	[kg]
m	=	total butterfly mass	[kg]
$\stackrel{P}{\hat{r}_2}$	=	power	[W]
\hat{r}_2	=	non-dimensional radius to the second moment of wing area, $\hat{r}_2 = r_2/R$	[1]
R	=	wing length	[m]
Re	=	Reynolds number, $Re = \rho_f U c_m / \mu$	[1]
S	=	wing area	$[m^2]$
St	=	Strouhal number, $St = 2fh_{a'}U$	[1]
T	=	thrust	[N]
t_*	=	time	[s]
t^*	=	non-dimensional time	[1]
U	=	freestream velocity	[m/s]
\ddot{w}	=	trailing edge vertical acceleration	$[m/s^2]$
$W_{\rm b}$	=	Average butterfly weight	[N]
α	=	pitch angle	[deg]
α_{a}	=	pitch amplitude	[deg]
α_{e}	=	end-of-stroke passive pitch angle	[deg]
α_{eff}	=	effective angle of attack	[deg]
α_{m}	=	mid-stroke passive pitch angle	[deg]
β	=	stroke plane angle	[deg]
γ	=	peak to peak flapping amplitude	[deg]
η	=	propulsive efficiency, $\overline{C_L}$ / $\overline{C_P}$	[1]
φ	=	phase offset between pitch and plunge motion	[deg]
ρ_{f}	=	air density	$[kg/m^3]$
$\rho_{\rm s}$	=	wing density	$[kg/m^3]$
ρ*	=	density ratio, $\rho^* = \rho_s/\rho_f$	[1]
μ	=	dynamic viscosity coefficient	[kg/m-s]

II. Introduction

IGRATION of Monarch butterflies is the longest among insects. Each year hundreds of millions of Monarch butterflies fly 4000 km during the fall [1–3]. This incredible journey remains a mystery even to this day. The physical understanding of the aerodynamic mechanism behind long range migration of Monarchs is currently underexplored.

During migration, glider pilots have spotted Monarch butterflies at an altitude of 1200 m [4]. At these high altitudes, the Monarch can take advantage of favorable weather and wind patterns in the boundary layer of the earth [3,5,6], presumably to conserve energy [7,8]. Additionally, all of their overwintering sites in Mexico are located at altitudes between 2900 m and 3200 m [9–13]. This high-altitude forest ecosystem is believed to lower their metabolic rates [3,14].

At an altitude of 3000 m, the air density ρ_f is only about 76% compared to the density at sea level [15]. At higher altitudes, Monarchs experience reduced aerodynamic drag forces due to lower air density, which can help in long-range flight. However, the aerodynamic lift which is required to stay aloft also should reduce at high altitudes due to reduced density. The lift generation mechanism in Monarchs essential for high-altitude long-range flight of Monarchs is inadequately understood.

One of the main effects of flying in a lower density environment is that the operating Reynolds number reduces. Monarch butterflies in general operate at Reynolds number $Re = \rho_f U c_m / \mu = O(10^3)$, based on the reference velocity U, average wing chord length c_m , and dynamic viscosity of air μ . In our recent free flight measurements of Monarch

butterflies at simulated altitudes between 193 m and 4500 m, the Reynolds number was Re = 3326, based on average thorax velocity and mean chord length of considered butterfly specimens and air density of $\rho_f = 1.2 \text{ kg/m}^3$.

Another effect of the reduced density is that the fluid-structure interaction (FSI) of the Monarch wings can change. Monarch butterflies have a large pairs of wings compared to their body. The large wings undergo significant deformation during flight. The shape variations associated with wing deformation directly affect the aerodynamic performance through a change in the effective angle of attack [16], resulting in load lifting capabilities [17]. Compliant wings are also shown to contribute in power reduction [18–21]. For example, wing deformations of locusts and hawkmoths have been shown to enhance the force generation and improve aerodynamic efficiency [22–24]. One of the key non-dimensional parameters characterizing the FSI of flapping wings is the density ratio $\rho^* = \rho_s/\rho_f$, the ratio between the wing density ρ_s and the surrounding fluid density ρ_f , which changes from 1.2 kg/m³ to 0.909 kg/m³ between 193 m and 3000 m.

The objective of the current study is to investigate the effects of decreasing air density on the aeroelastic performance of a flexible flapping wing at the Monarch scale. The lift, thrust, and power are calculated in a design space with varying air density ρ_f and stroke plane angle β of the wing. A two-dimensional motion of a chordwise flexible wing in a constant freestream flow with an imposed plunge at the leading edge of the wing is considered. A constant plunge amplitude h_a and frequency f are considered. The morphological and kinematic variables based on the experimental measurements are used as input parameters in the current study. The structural properties of the butterfly wing are determined using a high resolution micro-CT scan of the wing and from linear FEM analysis.

The interaction between the unsteady, viscous flow and the structural dynamics is solved by using a well validated aeroelastic framework [21,25–29]. For FSI, we focus on the chordwise flexibility. Flexural stiffness of insect wings varies differently along the spanwise and chordwise directions [30]. Typically, the chordwise wing stiffness is lower (i.e. more flexible) and directly affects aerodynamic performance through effective angle of attack [16]. The butterfly wing is considered as an elastic flat plate [21,30] and a plunge motion is prescribed at the leading edge of the plate to represent the leading edge vein [31].

The paper is organized as follows. We define the key morphological, structural, and kinematic parameters relevant to Monarch butterflies in Sections III.A and III.B. The governing equations for fluid and structural dynamics and the computational setup are discussed in Sections III.D and III.E. In Section III.F, we present the grid and timestep sensitivity results for a pitching and plunging wing at a representative Monarch butterfly Reynolds number of Re = 3437. Next, a discussion of the FSI at Monarch scale on a two-dimensional design space as a function of air density and stroke plane angle is presented.

III. Methodology

A. Morphological and Structural Parameters of Monarch Butterflies

Monarch butterflies have a pair of relatively large fore and hind wings (Fig. 1) which undergo large displacements during flight. The wings have veins embedded in them which run along spanwise and chordwise directions and give the wings directional stiffness.

We define the fore wing length R as the distance between the wing root and the wing tip (Fig. 1(a)). The total wing area S is defined as the area of all four wings in the overlapped configuration. The mean chord $c_{\rm m}$ is calculated as $c_{\rm m} = S/(2R)$. The non-dimensional radius to the second moment of wing area for the forewing is $\hat{r}_2 = r_2/R$, where r_2 is the second moment of wing area. We measured these morphological parameters for eight Monarch butterfly specimens. The Monarch butterflies were purchased from Swallowtail Farms [32]. Their average morphological parameters are summarized in Table 1 and are considered in this study

The structural parameters of the Monarch butterfly forewing were determined from a representative butterfly specimen. We performed a high resolution micro-CT scan of a forewing at 10 μ m resolution [33]. The details related to the processing of the micro-CT data is discussed in [33]. These micro-CT scan results show that the thickness h_s of the forewing membrane along the chordwise direction at around 20% R is 54×10^{-6} m and the volume of the wing is $V_w = 48.17 \times 10^{-9}$ m³. The wing density $\rho_s = 307$ kg/m³ was calculated from the mass of the forewing and the volume. The elastic modulus E of the wing in the chordwise direction was determined using a force-deflection experiment with a linear FEM analysis in [33]. The average E from five measurements was $E = 0.2 \times 10^9$ N/m². The structural parameters of the butterfly forewing are summarized in Table 2.

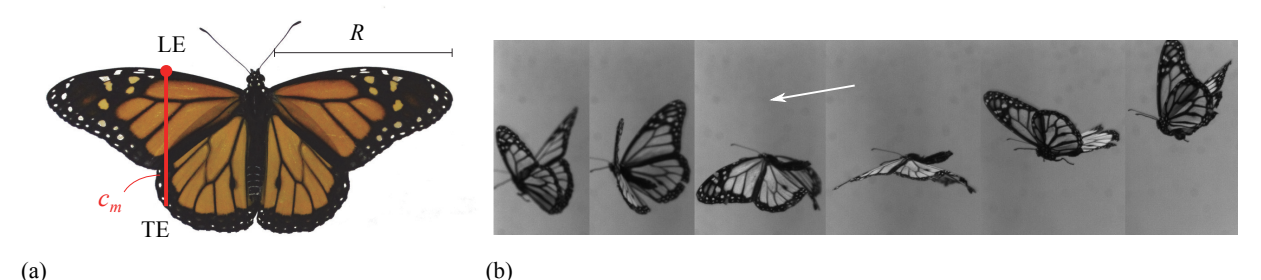


Fig. 1. (a) Monarch butterfly morphological parameters [34]. Red dot corresponds to leading edge of the wing. (b) High speed video snapshots of Monarch butterfly in free flight. Wings undergo significant deformation during flight.

Table 1. Morphological parameters considered in the current study. Each parameter is averaged over 8 butterfly specimens.

Parameter	Value
Total butterfly mass, <i>m</i> (kg)	0.5×10^{-3}
Forewing length, R (m)	57×10^{-3}
Total wing area, $S(m^2)$	34×10^{-4}
Non-dimensional radius to the second moment of wing area, \hat{r}_2	0.56
Mean chord, $c_{\rm m} = S/(2R)$ (m)	30×10^{-3}
Wing loading, mg/S (N/m ²)	1.44

Table 2. Structural parameters considered in the current study. The structural parameters of the forewing are measured for a single representative butterfly specimen [33].

Parameter	Value
Membrane thickness, h_s (m)	54×10 ⁻⁶
Wing density, $\rho_s (kg/m^3)$	307
Young's modulus, $E(N/m^2)$	0.2×10^9

B. Kinematic Parameters

We consider a two-dimensional plunge motion of a chordwise flexible wing as shown in Fig. 2. A sinusoidal plunge motion h with amplitude h_a and frequency f is imposed on the leading-edge (LE) of the wing as a function of time t. The non-dimensional form of the plunge motion can be written as

$$h^*(t^*) = St (\cos(2\pi t^*) - 1), \tag{1}$$

where $t^* = tf$ is the non-dimensional time and $St = 2fh_a/U$ is the Strouhal number and U is the reference velocity.

We experimentally measured the wing kinematics of freely flying Monarch butterflies using an optical measurement technique. The kinematic variables are calculated based on 22 experimentally measured free flights recorded between simulated altitudes of 193 m and 4500 m. The thorax velocity magnitude was calculated by differentiating the thorax position in time and was averaged over the length of each flight trajectory. The velocity magnitude varied between 0.77 m/s and 3.5 m/s with a mean velocity magnitude of 1.7 m/s. We consider a constant freestream velocity magnitude of U = 1.7 m/s in the current study. The flapping angle γ was found as the angle between the left and the right forewings. The flapping frequency f is determined from the Fast Fourier Transform (FFT) of the time history of the flapping angle. The average flapping amplitude and flapping frequency were $\gamma_{p2p} = 313$ deg and f = 10 Hz, respectively. We calculated the plunge amplitude at the \hat{r}_2 location based on the average peak-to-peak flapping amplitude γ_{p2p} , average wing length R as $h_a = R\hat{r}_2\sin(\gamma_{p2p}/4)$. The plunge amplitude varied between $h_a = 30$ mm and $h_a = 32$ mm with an average of $h_a = 31$ mm. We consider a plunge amplitude of $h_a = 31$ mm in the current study. We determined the stroke plane angle β from the 22 free flights as the angle between the longitudinal body axis and the normal to the plane containing the wing tip positions during flight. The measured stroke plane angle varied between $\beta = 3.3$ deg and $\beta = 33$ deg with a mean stroke plane angle of $\beta = 17$ deg. The average kinematic variables are summarized in Table 3.

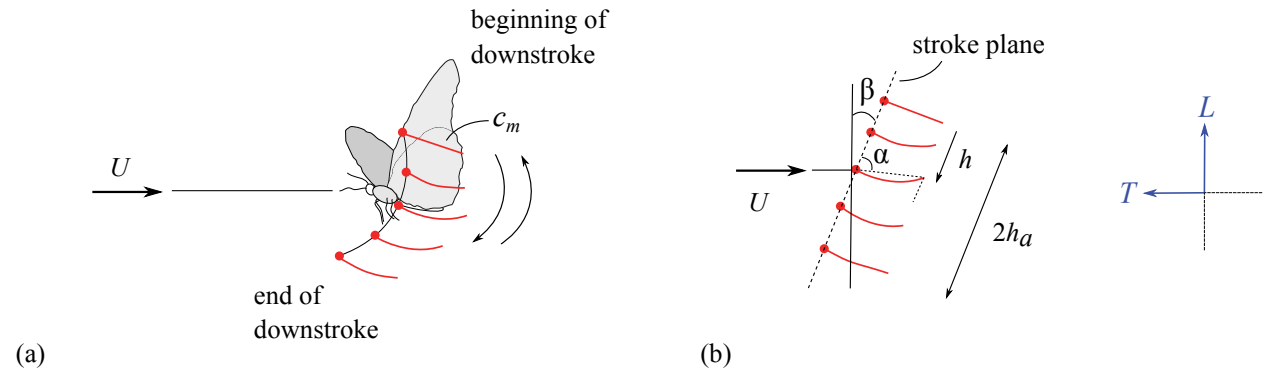


Fig. 2. (a) Schematic showing the flapping wing motion and the (b) corresponding plunge motion with an amplitude of h_a . Lift and thrust directions are indicated relative to the freestream direction. Passive pitch angle is denoted by α .

Table 3. Average kinematic variables calculated from experimental free flight measurements.

Kinematic variable	Value
Freestream velocity, U (m/s)	1.7
Flapping frequency, $f(Hz)$	10
Peak-to-peak flapping amplitude, γ_{p2p} (deg)	313
Plunge amplitude, h_a (mm)	31
Stroke plane angle, β (deg)	17

C. Design Space and Non-dimensional Parameters

Figure 3(a) shows the variation of air density with increase in altitude [15]. Monarchs encounter varying altitudes during their long range migration. In addition to flying at sea level conditions, Monarch butterflies fly at higher altitudes [4] and have been spotted at around 1200 m above sea level. Figure 3(a) shows the various altitudes at which migrating Monarchs are spotted as reported by Gibo [4]. Furthermore, the overwintering mountains in Central Mexico where Monarchs gather in millions are located at altitudes between 2900 m and 3200 m [9–13].

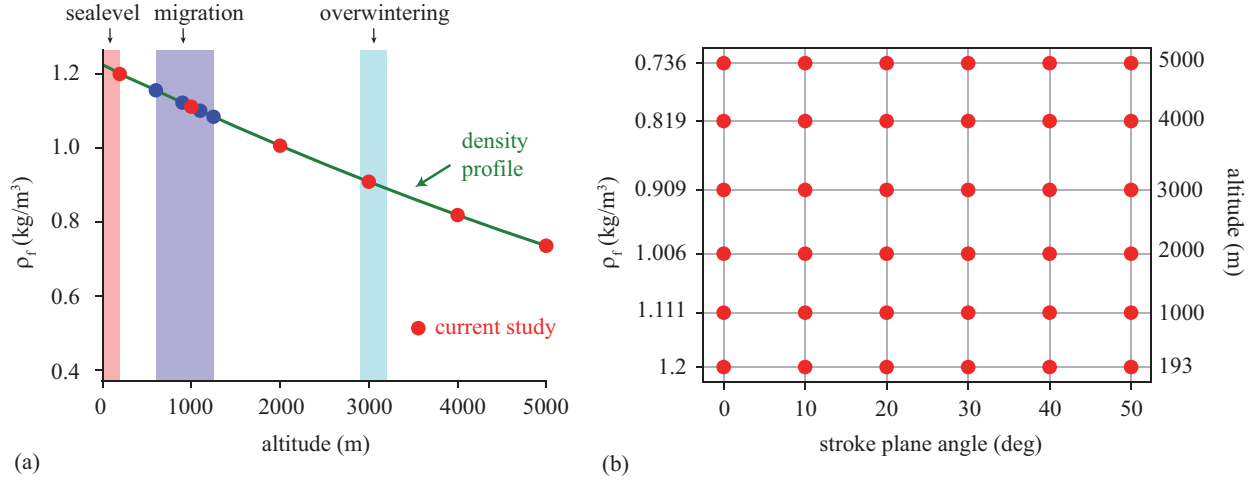


Fig. 3. Design space set up. (a) Air density variation with altitude. Red dots indicate the altitudes considered in the current study. The flight altitudes at which Monarchs were spotted [4] are shown as blue dots. (b) Two-dimensional design space with design variables air density ρ_f and stroke plane angle β . A uniform grid distribution is considered.

In this study, we consider a design space (Fig. 3(b)) with the air density ρ_f and the stroke plane angle β chosen as the design variables to assess the effects of altitude on the aerodynamic performance at Monarch butterfly scale. Six altitudes were considered between 193 m and 5000 m. The corresponding air density at these altitudes varies between $\rho_f = 1.2 \text{ kg/m}^3$ and $\rho_f = 0.736 \text{ kg/m}^3$. We consider six stroke plane angles between $\beta = 0$ deg and $\beta = 50$ deg

with 10 deg increments. The resulting design space consists of 36 design points. The plunge amplitude, plunge frequency and freestream velocity are kept constant in this study. The structural parameters are not varied in this study.

We characterize the flapping wing aerodynamics in forward flight by four non-dimensional variables [35]: Reynolds number Re, Strouhal number St, reduced frequency $k = \pi f c_m/U$, and stroke plane angle β . The Reynolds number describes the relative importance of fluid inertia and viscous effects. The Strouhal number compares the velocity of the wing tip to the forward flight of the butterfly. Finally, reduced frequency characterizes the unsteadiness in the flow field. In the considered altitude range between 193 m and 5000 m (Fig. 3), the Reynolds number varies between Re = 3326 and Re = 2040 due to change in air density. The Strouhal number remains constant at St = 0.36 and the reduced frequency is also constant at k = 0.55 in this study.

Additional dimensionless parameters arise when a flexible wing is considered [21]. The three key non-dimensional structural parameters are the density ratio ρ^* , thickness ratio h_s^* , and the frequency ratio f/f_1 . The density of air varies between 1.2 kg/m³ and 0.736 kg/m³ between the considered altitude range of 193 m and 5000 m [15]. The measured density of Monarch wings was 307 kg/m³ (Section III.A). As a result, the density ratio varies between $\rho^* = 256$ and $\rho^* = 417$. The thickness ratio $h_s^* = h_s/c_m$ is the wing thickness normalized by the mean chord. The thickness ratio calculated based on wing membrane thickness was $h_s^* = 1.8 \times 10^{-4}$ (Table 4). Finally, the frequency ratio, f/f_1 , defined as the ratio of the flapping frequency f and the first natural frequency of the wing in chordwise direction, f_1 , is $f/f_1 = 1.28$. The non-dimensional parameters are summarized in Table 4.

Table 4. Non-dimensional variables at the Monarch butterflies scale considered in the current study.

Non-dimensional variable	Value		
Reynolds number, $Re = \rho_f U c_m / \mu$	3326 - 2040		
Reduced frequency, $k = \pi f c_m / U$	0.55		
Strouhal number, $St = 2fh_a/U$	0.36		
Thickness ratio, $h_s^* = h_s/c_m$	1.8×10^{-4}		
Density ratio, $\rho^* = \rho_s/\rho_f$	256 - 417		
Frequency ratio, f/f_1	1.28		
Stroke plane angle, β (deg)	0 - 50		

D. Governing Equations

The flow field is governed by the unsteady Navier-Stokes equations with constant density ρ_f and viscosity μ ,

$$\nabla^* \cdot \mathbf{u}^* = 0$$

$$\frac{k}{\pi} \frac{\partial \mathbf{u}^*}{\partial t^*} + (\mathbf{u}^* \cdot \nabla^*) \mathbf{u}^* = -\nabla^* p^* + \frac{1}{Re} \Delta^* \mathbf{u}^*$$
(2)

for the velocity \mathbf{u} , pressure p, and time t. The superscript (*) indicates dimensionless variables. The dimensional variables are non-dimensionalized with a freestream velocity U, inverse of the motion frequency 1/f, and chord c, respectively.

We consider a two-dimensional, elastic wing structure with uniform thickness h_s , density ρ_s , and elastic modulus E. As the flat plate follows the imposed vertical motion, Eq. (1), at the LE, the resulting fluid dynamic force dynamically balances with the wing inertia and the elastic bending forces, modeled locally as a linear Euler-Bernoulli beam [30] as

$$\frac{\partial^2 w^*}{\partial t^{*2}} + \frac{4\pi^2}{k_1^4} \left(\frac{f_1}{f}\right)^2 \frac{\partial^4 w^*}{\partial x^{*4}} = \frac{p^*}{h_*^* \rho^*} \left(\frac{\pi}{k}\right)^2, \tag{3}$$

where $w^* = w/c$ is the displacement due to bending motion, f/f_1 is the frequency ratio, and $k_1 = 1.875$ is the first root corresponding to first natural frequency of the wing.

The resulting wing camber deformations $(w-h)/c_m$ can also be regarded as a pitch rotation $\alpha(t^*)$, the angle between the trailing-edge (TE) and LE, see Fig. 2(b). Passive pitch angle acts as an effective angle of attack, measured in terms of the angular amplitude α_a and the phase lag φ . To characterize the pitch angle, we use the pitch amplitude α_a and phase φ by approximating the pitch by a first-order harmonic as

$$\alpha_{FH} = 90^{\circ} - \alpha_a \cos(2\pi t^* + \varphi). \tag{4}$$

We determine the wing deformations at the TE of the wing at the middle and the end of the strokes, $v_m = v^*(0.25)$ and $v_e = v^*(0.5)$, where again v = w - h is the wing deformation relative to the imposed plunge motion h at the LE. The relative wing deformations are converted to passive pitch angles α as $\alpha_m = \arctan(v_m)$ and $\alpha_e = \arctan(v_e)$. Based on these two angles, a first-order harmonic approximation can be constructed for the passive pitch, Eq. (4), by solving for the phase lag φ and the angular amplitude α_a with $\alpha_{FH}(0.25) = \alpha_m$ and $\alpha_{FH}(0.5) = \alpha_e$.

The effective angle of attack is a key aerodynamic parameter and is defined based on the instantaneous plunge motion and the passive pitch as

$$\alpha_{\text{eff}}(t) = -\arctan\left(\frac{w(t) - h(t)}{c_m}\right) - \arctan\left(\frac{\dot{h}(t)}{U}\right) + \beta. \tag{5}$$

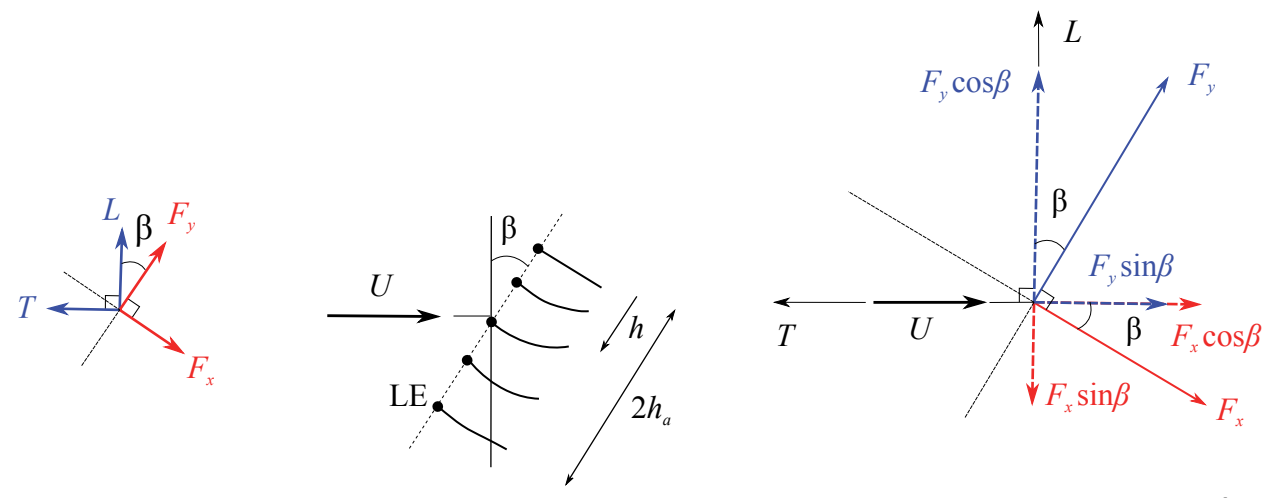


Fig. 4. Plunge motion and definitions of lift and thrust relative to the freestream U and stroke plane angle β .

The aerodynamic performance is evaluated using three key quantities: lift, thrust and power. The lift and thrust are calculated using the horizontal and vertical force components at a given stroke plane angle β (Fig. 4) as

$$L = 2R(F_y \cos \beta - F_x \sin \beta)$$

$$T = -2R(F_y \sin \beta - F_x \cos \beta),$$
(6)

where F_x and F_y are the horizontal and vertical components of force per unit span, respectively, L and D are the lift and thrust (Fig. 4) which are perpendicular and parallel to the freestream direction, respectively.

We avoid the initial transients and carry out the time averaging over the second motion cycle. The time-averaged lift for example is defined as

$$\overline{L} = \int_{T}^{2T} L(t)dt, \tag{7}$$

The time-averaged lift and thrust coefficients are defined as

$$\overline{C}_{L} = \frac{\overline{L}}{\frac{1}{2}\rho_{f}U^{2}c_{m}}, \qquad \overline{C}_{T} = \frac{\overline{T}}{\frac{1}{2}\rho_{f}U^{2}c_{m}}, \qquad (8)$$

To measure the cost of performance, we define the time-averaged power as

$$\overline{P} = -2R \int_{T}^{2T} F_{y}(t) \dot{h}(t) dt - 2R \int_{T}^{2T} \dot{h}(t) \int_{LE}^{TE} \rho_{s} h_{s} \ddot{w}(t) dx dt,$$

$$\tag{9}$$

The second term in the above equation represents the inertial power associated with the wing motion.

E. Numerical Models and Computational Setup

The aerodynamic forces and moments are calculated directly by the coupled Navier–Stokes equations (Eq. (2)) and structural dynamics solvers (Eq. (3)) under the imposed kinematics (Eq. (1)), by integrating the pressure and shear forces on the wing. We use an in-house, structured, pressure-based finite volume solver to solve for Eq. (2) that governs the motion of the fluid [21,25,26,29]. The convection terms are discretized using a second-order upwind scheme, and the pressure and viscous terms are treated with second-order central difference schemes. An implicit Euler scheme is used for time integration.

We solve Eq. (3) using a finite element representation of the Euler–Bernoulli beam model. The wing is modeled by a flat plate with 51 equally distributed nodes. The two degrees of freedom included in the model are the transverse displacement and bending. For qualitative investigation of the flexible flapping wing aeroelasticity, a linear Euler–Bernoulli beam model was shown to be sufficient for a chordwise flexible airfoil [21]. Radial basis function interpolation is used to deform the mesh [36].

The governing Eqs. (2) and (3) for the fluid and structure, respectively, are solved independently. The fluid-structure interaction coupling is a time-domain partitioned process. At each time step the fluid and structural solutions are iterated until sufficient convergence is reached for the displacement of the flexible wing within an inner-iteration before advancing to the next time step. Details of the fluid-structure interaction and careful validation studies against well-documented experimental results are shown in our previous work [21,25,26].

The computational domain is shown in Fig. 5(a) with a $0.02c_m$ thick flat plate at the center of the domain with the outer boundary located at a radial distance of $100c_m$. The mesh is extruded by unit distance along the z-direction. We impose a freestream velocity at the inlet of the computational domain as shown in Fig. 5(a). A no-slip condition is imposed on the flat plate surface. A fixed zero-pressure condition is set at the outlet boundary. The time step and grid sensitivity tests as well as the details of the computational setup are discussed in Section III.F.

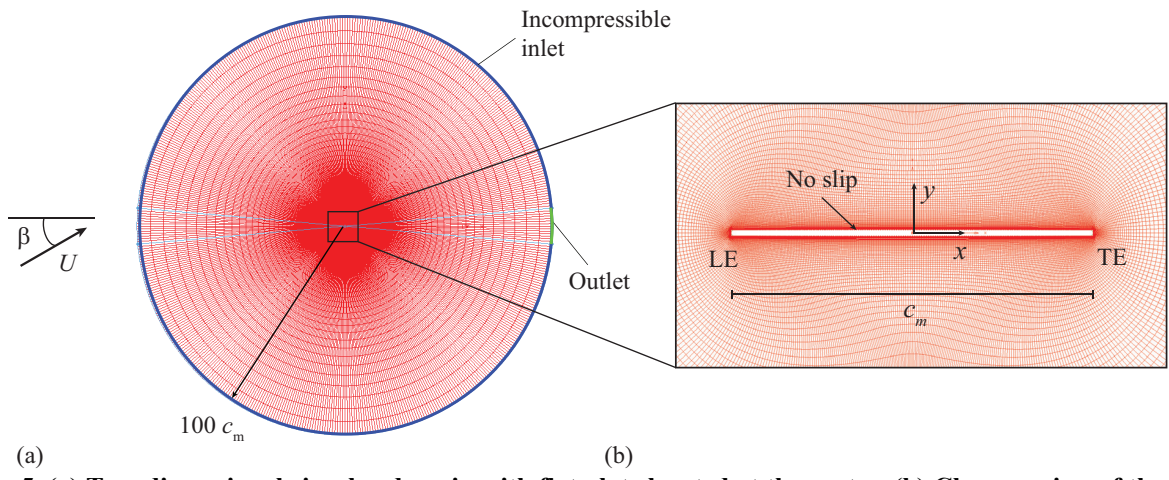


Fig. 5. (a) Two-dimensional circular domain with flat plate located at the center. (b) Close up view of the grid around the flat plate. Incompressible inlet boundary condition is prescribed at the inlet with freestream velocity U = 1.7 m/s and no-slip boundary condition on the flat plate. The outer boundary is located at a radius of $100c_{\rm m}$ from the domain center.

F. Grid Convergence and Timestep Sensitivity Study

We conducted a grid and timestep sensitivity study with a rigid pitching and plunging wing at Re = 3437, k = 0.57, and St = 0.47 at a stroke plane angle of $\beta = 0$ deg. We used a representative pitch and plunge motion to assess the grid and time step sensitivity. The sinusoidal pitch had an amplitude of 45 deg, phase lag of 90 deg, and pitch

axis was located at center of the flat plate. We prescribed a plunge amplitude of 40 mm. Five levels of grids were considered with 61 to 481 points on the wing (Table 5). A freestream velocity of U = 1.7 m/s was prescribed at the domain inlet as shown in Fig. 5(a). For each grid level, we calculated L_2 norm of thrust coefficients for two flapping cycles between $t^* = 1$ and $t^* = 2$ with solution at extra fine grid considered as the most accurate solution.

Table 5. Summary of grid sensitivity results for two-dimensional rigid wing computation. The L_2 norm of

mean thrust coefficient is reported based on two flapping periods.

	Grid type	Points on the wing	Total cells in the domain	L_2 Norm, $\overline{C_T}$
	Coarse	31	5950	10.256
Grid	Medium	61	13736	7.287
sensitivity	Fine	121	34584	4.053
sensitivity	Very Fine	241	70104	2.08
	Extra Fine (baseline)	481	156058	-

Figure 6 shows the variation of thrust coefficient (Eq. (8)) for all the grid levels. The thrust coefficients shows periodic variation. The thrust coefficient is always positive indicating that the wing motion generates positive thrust. The L_2 norm of thrust coefficient for three flapping cycles shown in Table 5 also indicate that grid convergence is achieved based on a grid with 241 points on the wing. Based on Fig. 6 and Table 5, the grid with 241 points on the wing was chosen as the optimal grid for all computations.

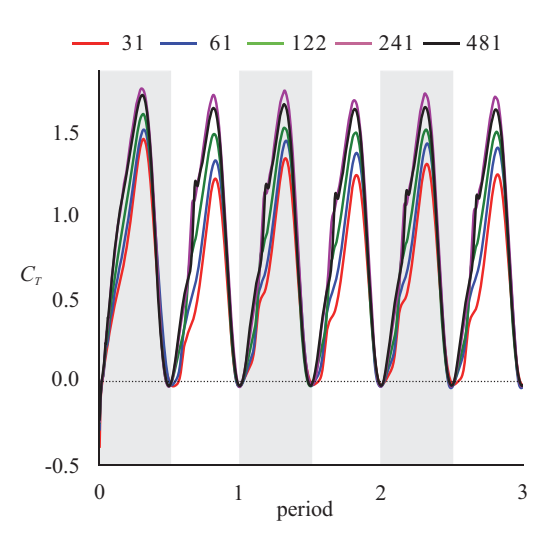


Fig. 6. Grid convergence study for two-dimensional rigid wing motion for five different grid levels. Time history of thrust coefficient for three flapping periods. The grid sensitivity results are summarized in Table 5.

Timestep sensitivity was performed similarly with the converged grid with 241 points on the wing. We considered four timesteps levels as shown in Table 6. For each timestep, we calculated the L_2 norm of the thrust coefficient for two flapping cycles between $t^* = 1$ and $t^* = 2$ with solution at 960 time steps per motion cycle considered as the most accurate solution (Table 6). The C_T profiles show minimal variation with different timesteps. The timestep of $\Delta t = 2.083 \times 10^{-4}$ s was chosen as the optimal timestep for all computations and it corresponds to 480 timesteps per flapping cycle.

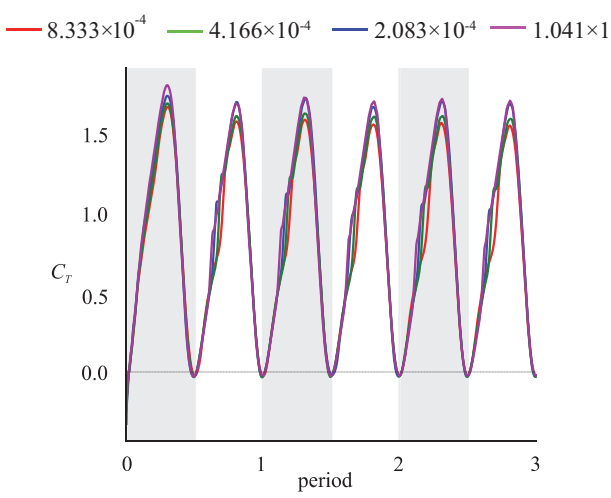


Fig. 7. Timestep sensitivity study for two-dimensional rigid wing motion with baseline grid with 241 points on the flat plate for four different timesteps. Time history of thrust coefficient for three flapping cycles is shown. The timestep sensitivity results are summarized in Table 6.

Table 6. Timestep sensitivity results for the baseline grid. The L_2 norm of mean thrust coefficient is reported

based on two flapping periods.

	Time steps per cycle	Timestep, Δt (s)	L_2 Norm, $\overline{C_T}$
	120	8.333×10^{-4}	2.108
Timestep	240	4.166×10^{-4}	2.09
sensitivity	480	2.083×10^{-4}	1.681
	960 (baseline)	1.041×10^{-4}	-

IV. Results and Discussion

A. Lift, Thrust, and Power Required

Figure 8 shows the mean aerodynamic response obtained using flexible wings in the design space (see Section III.F) with respect to the changes in the air density and stroke plane angle.. The variation of mean lift in the design space is shown in Fig. 8(a). All wing motions generate positive mean lift at all altitudes. At lower stroke plane angles, where the wing motion is nearly normal to the freestream, the mean lift is close to zero. We see an increase in lift as the stroke plane angle increases. The mean lift does not vary significantly with altitude at lower stroke plane angles. However, the effects of altitude on the mean lift become more pronounced as the stroke plane angle increases. The equilibrium lift required to maintain the average butterfly weight is $W_b = 4.8$ mN, indicated by a black solid line in Fig. 8(a). To generate sufficient lift for a butterfly to stay aloft, a relatively high stroke plane angle is required, especially at higher altitudes. The mean lift drops gradually when altitude is higher than 3000 m.

The mean thrust is much lower in magnitude in the design space as shown in Fig. 8(b). At lower altitude and lower stroke plane angle motions, positive thrust is generated. In general, the mean thrust decreases with increase in both altitude and stroke plane angle. At higher altitudes and stroke plane angles, the mean thrust becomes negative, indicating that there is drag, albeit with a small magnitude.

The mean aerodynamic power (Eq. (9)) variation in the design space is shown in Fig. 8(c). In general, the power required reduces with the altitude and stroke plane angle. A negative power consumption is an indication that the power is extracted from the surrounding fluid [37]. Occurrence of negative aerodynamic power was also reported for aeroelastic response in forward flight at bird scales [38].

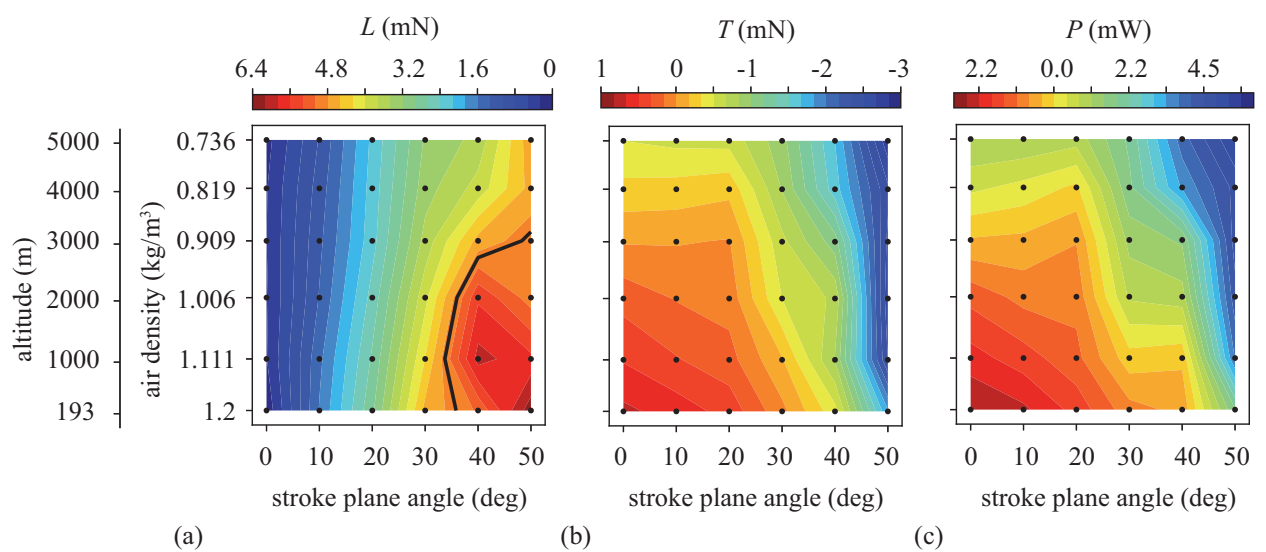


Fig. 8. Mean (a) lift (b) thrust and (c) power with respect to the changes in the air density and stroke plane angle. The equilibrium butterfly weight $W_b = 4.8$ mN is shown in (a) with a solid black line. The design points are shown as black dots.

B. Passive Pitch, Phase Lag, and Effective Angle of Attack

The variation of key structural parameters with altitude and stroke plane angle is shown in Fig. 9. The passive pitch amplitude, phase lag, and effective angle of attack are shown in Fig. 9 as a function of altitude (Fig. 9(a-c)) and stroke plane angle altitude (Fig. 9(d-f)).

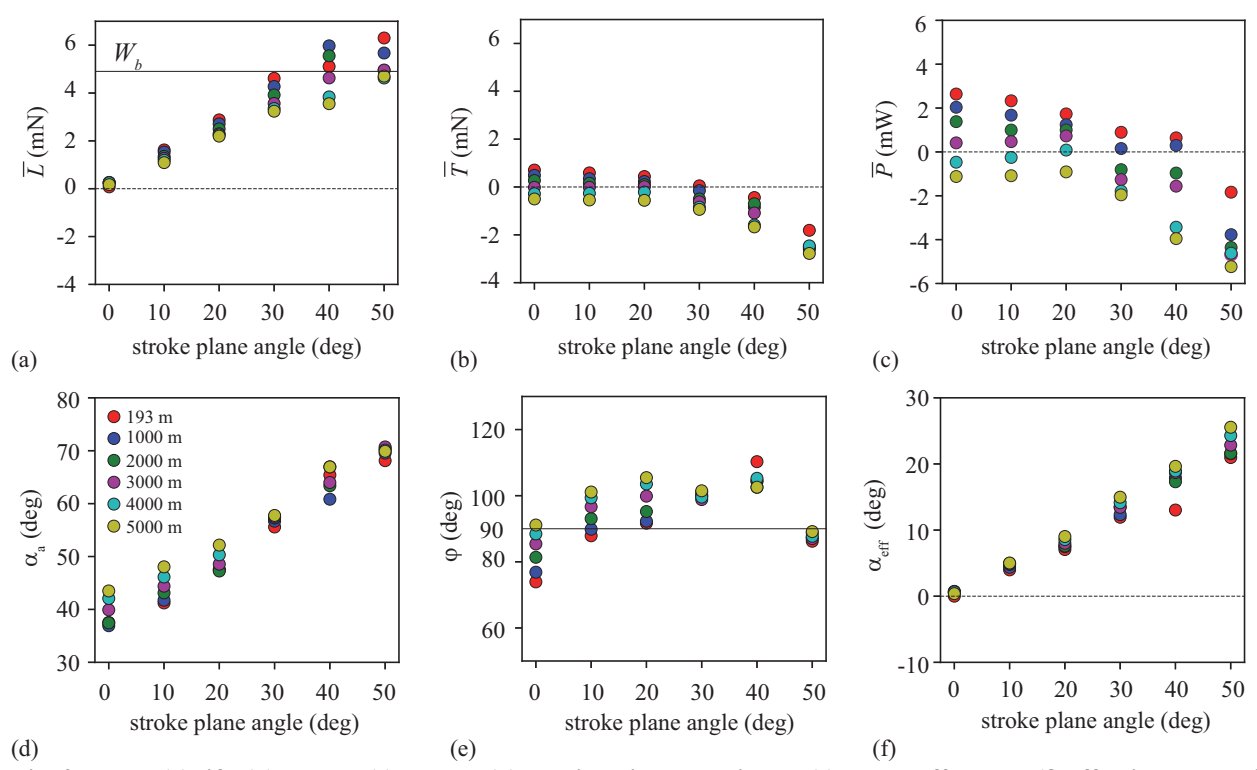


Fig. 9. Mean (a) lift, (b) thrust, (c) power, (d) passive pitch amplitude, (e) phase offset and (f) effective angle of attack with respect to the changes in the air density and stroke plane angle.

The angular amplitude varies between 38 deg and 71 deg as shown in Fig. 9(a). In general, the angular amplitude increases with the stroke plane angle (Fig. 9(d)). For a given stroke plane angle, the passive pitch amplitude increases with the altitude. A highest amplitude of 71 deg is observed at $\beta = 50$ deg and at altitude of 3000 m in Fig. 9(a).

The phase lag φ measures the delay between the TE position and the imposed plunge motion at the LE due to passive pitch wing deformation. A zero stroke plane angle results in a phase lag with φ < 90 deg at lower altitudes (Fig. 9(b)) and the phase lag becomes 90 deg at the highest altitude. At higher stroke plane angles, the phase lag remains nearly 90 deg at all altitudes. The phase lag is higher than 90 deg for intermediate stroke plane angles between β = 20 deg and 40 deg (Fig. 9(e)).

The effective angle of attack varies between 0 deg and 26 deg in the design space (Fig. 9(c)). The effective angle of attack, which includes the effects of the passive pitch, plunge velocity, and stroke plane angle, is nearly zero at a zero stroke plane angle. With increase in the stroke plane angle we observe higher effective angle of attack (Fig. 9(f)), compensating for the reduction due to passive pitch. At β = 50 deg and 193 m altitude the effective angle of attack is α_{eff} = 21 deg whereas at 5000 m α_{eff} = 26 deg. At a given stroke plane angle, α_{eff} is higher at higher altitudes.

C. Lift, Thrust and Power Coefficients

Lift coefficient varies nearly linearly with effective angle of attack up to $\alpha_{\rm eff} = 17$ deg (Fig. 10(a)). Between $\alpha_{\rm eff} = 17$ deg and $\alpha_{\rm eff} = 25$ deg, the trend is nonlinear. A peak $\overline{C_L}$ of 0.7 is observed at $\alpha_{\rm eff} = 25$ deg which corresponds to an altitude of 5000 m and $\beta = 50$ deg. The lift curve slope was $d\overline{C_L}/d\alpha_{\rm eff} = 2.36$ between 0 deg and 17 deg.

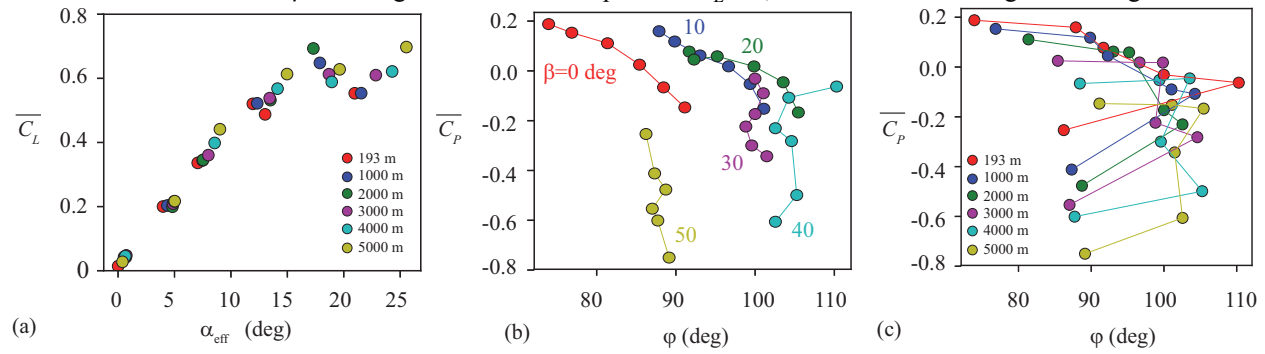


Fig. 10. Variation of mean (a) lift coefficient with effective angle of attack. Variation of mean power coefficient with phase lag (b) colored by stroke plane angles (c) colored by altitude.

Figure 10(b,c) shows the variation of mean power coefficient with the phase lag. For a given stroke plane angle, a reduction in the air density (higher altitudes) results in a lower power coefficient. For stroke plane angles of $\beta = 0$, 10, 20, and 50 deg, higher altitudes yield a greater phase lag. For stroke plane angles of $\beta = 30$ deg, the trend is nonlinear. Figure 10(c) shows that the relation between $\overline{C_P}$ and φ is a reversed C type, showing a peak in φ at midaltitudes.

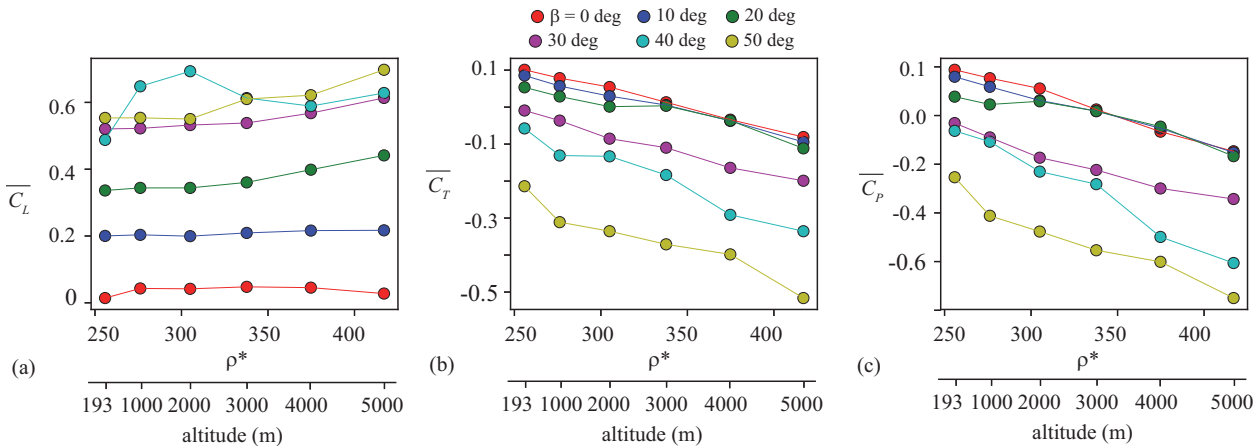


Fig. 11. Variation of cycle averaged lift, thrust and power coefficients with density ratio.

Figure 11 shows the variation of the lift, thrust, and power coefficients with respect to the density ratio. In general, thrust and power coefficients reduce with the altitude. The lift coefficient shows a more complicated trend with the highest lift coefficient of 0.7 reached at $\rho^* = 417$ (altitude 5000 m) for $\beta = 50$ deg.

D. Effects of High Altitude Density Conditions on the Monarch Flight

During the long distance migration and overwintering, Monarch butterflies navigate at varying altitude conditions: they are seen to migrate at 1200 m and overwinter at 3000 m. Between 193 m and 3000 m, the density of the air decreases by about 25% from 193 m (1.2 kg/m³) to 3000 m (0.91 kg/m³). Because aerodynamic forces are proportional to air density, one of the main benefits of flying at higher altitudes is reduced drag that enhance the flight range and endurance. In spite of the decrease in density, this study shows that Monarchs can increase the stroke plane angle to produce sufficient lift to stay aloft without paying a penalty in drag and required power. In fact, the power required reduces with the altitude, eventually becoming negative at 3000 m. When power required becomes negative, the wing motion extracts energy from the surrounding fluid [37], implying that no active energy expenditure is required to sustain the wing motion.

V. Concluding Remarks

In this study, we evaluated the effects of varying density on the aeroelastic wing response at Monarch butterfly scale. The air density and stroke plane angles were considered as design variables. We considered a range of air densities corresponding to altitudes that are relevant for Monarchs during their long range migration. We considered the effects of chordwise flexibility by coupling Navier-Stokes solver with a structural dynamics solver and determined the aerodynamic and structural response at Monarch scale under a constant freestream flow.

Our results show that mean lift reduces with altitude as expected but increases with the stroke plane angle. The drag remains nearly zero at all altitudes, although it increases slightly with the stroke plane angle. The power required decreases with altitude. The increase of lift with stroke plane angle can be attributed to the increase in the effective angle of attack which represents a combined angle due to passive pitch, the angle of attack due to plunge motion and the stroke plane angle. Finally, we observe negative power at higher altitudes which indicates no active energy expenditure is required to sustain the wing motion.

Our objective in this study was to test the hypothesis that the higher altitudes offer enhanced aerodynamic benefits for Monarch flight. Although the lift production reduces with altitude, the stroke plane angle can be modulated without too much penalty in power requirements. The power consumption substantially benefits from flying at higher altitudes. At lower altitudes near sea level, Monarchs can leverage the relatively large magnitude of their lift and thrust forces. At higher altitudes butterflies aim to minimize the power.

Note that this study considers an abstracted model of the more complicated Monarch flight: Current study is based on two-dimensional chordwise flexible wing whereas the butterfly flight is actually three-dimensional with highly anisotropic wings. We prescribe a constant freestream flow while the experimental measurements shows the freestream velocity in free flight ranges between 0.77 m/s and 3.5 m/s. The elastic modulus of the wing was not varied while our experiments showed a range between 1.3×10^9 N/m² to 2.7×10^9 N/m². The variation in wing density that may involve between multiple wing specimens was not considered. Monarch free flight follows an undulating trajectory and in our previous study [34], we showed that the two-way coupled wing-body motion in Monarchs can results in power saving. We do not consider undulations in the current simulation. Nevertheless, this study shows the importance of the effects of fluid-structure interaction on aerodynamic performance with chordwise flexible wings at Monarch scale which are not captured by rigid wing models.

Acknowledgments

We thank the University of Alabama in Huntsville undergraduate students Clifford Tatum and Jared Sampson for processing butterfly measurements. We thank Rachel Twigg for providing Monarch butterfly structural parameters. This work is supported by NSF CMMI-1761618.

References

- [1] Merlin, C., Gegear, R. J., and Reppert, S. M., "Antennal Circadian Clocks Coordinate Sun Compass Orientation in Migratory Monarch Butterflies," *Science*, Vol. 325, Nr. September, 2009, pp. 1700–1705.
- [2] Brower, L. P., Fink, L. S., and Walford, P., "Fueling the Fall Migration of the Monarch Butterfly," *Integrative and Comparative Biology*, Vol. 46, Nr. 6, 2006, pp. 1123–1142.
- [3] Brower, L., "Monarch Butterfly Orientation: Missing Pieces of a Magnificent Puzzle," Journal of Experimental Biology,

- Vol. 199, Nr. 1, 1996, pp. 93-103.
- [4] Gibo, D. L., "Altitudes Attained by Migrating Monarch Butterflies, Danaus Plexippus (Lepidoptera: Danainae), as Reported by Glider Pilots," *Canadian Journal of Zoology*, Vol. 59, Nr. 3, 1981, pp. 571–572.
- [5] Taylor, L. R., "Insect Migration, Flight Periodicity and the Boundary Layer," *Journal of Animal Ecology*, Vol. 43, Nr. 1, 1974, pp. 225–238.
- [6] Gibo, D. L., and Pallet, M. J., "Soaring Flight of Monarch Butterflies, Danaus Plexippus (Lepidoptera: Danaidae), During the Late Summer Migration in Southern Ontario," *Canadian Journal of Zoology*, Vol. 57, Nr. 7, 1979, pp. 1393–1401.
- [7] Paoletti, P., and Mahadevan, L., "Intermittent Locomotion as an Optimal Control Strategy Subject Areas:," 2014.
- [8] Kovac, M., Vogt, D., Ithier, D., Smith, M., and Wood, R., "Aerodynamic Evaluation of Four Butterfly Species for the Design of Flapping-Gliding Robotic Insects," *IEEE International Conference on Intelligent Robots and Systems*, 2012, pp. 1102–1109.
- [9] Wassenaar, L. I., and Hobson, K. A., "Natal Origins of Migratory Monarch Butterflies at Wintering Colonies in Mexico: New Isotopic Evidence," *Proceedings of the National Academy of Sciences*, Vol. 95, Nr. 26, 1998, pp. 15436–15439.
- [10] Slayback, D. A., Brower, L. P., Ramirez, M. I., and Fink, L. S., "Establishing the Presence and Absence of Overwintering Colonies of the Monarch Butterfly in Mexico by the Use of Small Aircraft," *American Entomologist*, Vol. 53, Nr. 1, 2007, pp. 28–40.
- [11] Alonso-Mejía, A., Rendon-Salinas, E., Montesinos-Patiño, E., and Brower, L. P., "Use of Lipid Reserves by Monarch Butterflies Overwintering in Mexico: Implications for Conservation," *Ecological Applications*, Vol. 7, Nr. 3, 1997, pp. 934–947.
- [12] Urquhart, F. A., "Found at Last; the Monarch's Winter Home," *National Geographic Magazine*, Vol. 150, 1976, pp. 161–173.
- [13] Urquhart, F. A., and Urquhart, N. R., "The Overwintering Site of the Eastern Population of the Monarch Butterfly (Danaus Plexippus; Danaidae) in Southern Mexico," *Journal of the Lepidopterists' Society*, Vol. 30, Nr. 3, 1976, pp. 153–158.
- [14] Masters, A. R., Malcolm, S. B., and Brower, L. P., "Monarch Butterfly (Danaus Plexippus) Thermoregulatory Behavior and Adaptations for Overwintering in Mexico," *Ecology*, Vol. 69, Nr. 2, 1988, pp. 458–467.
- [15] NASA, U.S. Standard Atmoshpere, N77-16482: 1976.
- [16] Kang, C. K., and Shyy, W., "Scaling Law and Enhancement of Lift Generation of an Insect-Size Hovering Flexible Wing," *Journal of The Royal Society Interface*, Vol. 10, Nr. 85, 2013, pp. 20130361–20130361.
- [17] Mountcastle, A. M., Combes, S. a, and Mountcastle, A. M., "Wing Flexibility Enhances Load-Lifting Capacity in Bumblebees.," *Proceedings. Biological Sciences / The Royal Society*, Vol. 280, Nr. 1759, 2013, p. 20130531.
- [18] Eldredge, J. D., Toomey, J., and Medina, A., "On the Roles of Chord-Wise Flexibility in a Flapping Wing with Hovering Kinematics," *Journal of Fluid Mechanics*, Vol. 659, 2010, pp. 94–115.
- [19] Ramananarivo, S., Godoy-Diana, R., and Thiria, B., "Rather than Resonance, Flapping Wing Flyers May Play on Aerodynamics to Improve Performance," *Proceedings of the National Academy of Sciences*, Vol. 108, Nr. 15, 2011, pp. 5964–5969.
- [20] Vanella, M., Fitzgerald, T., Preidikman, S., Balaras, E., and Balachandran, B., "Influence of Flexibility on the Aerodynamic Performance of a Hovering Wing.," *The Journal of experimental biology*, Vol. 212, Nr. Pt 1, 2009, pp. 95–105.
- [21] Kang, C., Aono, H., Cesnik, C. E. S., and Shyy, W., "Effects of Flexibility on the Aerodynamic Performance of Flapping Wings," *Journal of Fluid Mechanics*, Vol. 689, 2011, pp. 32–74.
- [22] Walker, S. M., Thomas, A. L. R., and Taylor, G. K., "Deformable Wing Kinematics in Free-Flying Hoverflies.," *Journal of the Royal Society, Interface / the Royal Society*, Vol. 7, Nr. 42, 2010, pp. 131–142.
- [23] Young, J., Walker, S. M., Bomphrey, R. J., Taylor, G. K., and Thomas, A. L. R., "Details of Insect Wing Design and Deformation Enhance Aerodynamic Function and Flight Efficiency.," *Science*, Vol. 325, Nr. 5947, 2009, pp. 1549– 1552.
- [24] Nakata, T., and Liu, H., "Aerodynamic Performance of a Hovering Hawkmoth with Flexible Wings: A Computational Approach," *Proceedings of the Royal Society B: Biological Sciences*, Vol. 279, Nr. 1729, 2012, pp. 722–731.
- [25] Shyy, W., Aono, H., Chimakurthi, S. K., Trizila, P., Kang, C. K., Cesnik, C. E. S., and Liu, H., "Recent Progress in Flapping Wing Aerodynamics and Aeroelasticity," *Progress in Aerospace Sciences*, Vol. 46, Nr. 7, 2010, pp. 284–327.
- [26] Chimakurthi, S. K., Tang, J., Palacios, R., S. Cesnik, C. E., and Shyy, W., "Computational Aeroelasticity Framework for Analyzing Flapping Wing Micro Air Vehicles," *AIAA Journal*, Vol. 47, Nr. 8, 2009, pp. 1865–1878.
- [27] Bluman, J., and Kang, C. K., "Wing-Wake Interaction Destabilizes Hover Equilibrium of a Flapping Insect-Scale Wing," *Bioinspiration and Biomimetics*, Vol. 12, Nr. 4, 2017.
- [28] Bluman, J., and Kang, C., "Achieving Hover Equilibrium in Free Flight with a Flexible Flapping Wing," *Journal of Fluids and Structures*, Vol. 75, 2017, pp. 117–139.
- [29] Bluman, J. E., Sridhar, M. K., and Kang, C., "Chordwise Wing Flexibility May Passively Stabilize Hovering Insects," *Journal of Royal Society Interface*, Vol. 15, 2018, p. 20180409.
- [30] Combes, S. A., and Daniel, T. L., "Flexural Stiffness in Insect Wings. I. Scaling and the Influence of Wing Venation.," The Journal of experimental biology, Vol. 206, Nr. Pt 17, 2003, pp. 2979–2987.
- [31] Combes, S. A., and Daniel, T. L., "Flexural Stiffness in Insect Wings II. Spatial Distribution and Dynamic Wing

- Bending," Journal of Experimental Biology, Vol. 206, Nr. 17, 2003, pp. 2989–2997.
- [32] "Swallowtail Farms" Available: http://www.swallowtailfarms.com/.
- [33] Twigg, R., Sridhar, M. K., Pohly, J. A., Hilderbrant, N., Kang, C., Landrum, D. B., Rho, K.-H., and Salzwedel, S., "Aeroelastic Characterization of Real and Artificial Monarch Butterfly Wings," Orlando, FL: AIAA SciTech Forum, 2020.
- [34] Sridhar, M., Kang, C.-K., and Landrum, D. B., "Beneficial Effect of the Coupled Wing-Body Dynamics on Power Consumption in Butterflies," *AIAA Aerospace Sciences Meeting*, San Diego, CA: AIAA-2019-0566, 2019, pp. 1–12.
- [35] Shyy, W., Aono, H., Kang, C., and Liu, H., An Introduction to Flapping Wing Aerodynamics, Cambridge University Press, New York, 2013.
- [36] de Boer, A., van der Schoot, M. S., and Bijl, H., "Mesh Deformation Based on Radial Basis Function Interpolation," *Computers and Structures*, Vol. 85, Nr. 11–14, 2007, pp. 784–795.
- [37] Fung, Y. C., An introduction to the theory of aeroelasticity, Courier Dover Publications, 2008.
- [38] Kodali, D., Medina, C., Kang, C., and Aono, H., "Effects of Spanwise Flexibility on the Performance of Flapping Flyers in Forward Flight," *Journal of Royal Society Interface*, Vol. 14, 2017, p. 20170725.